

TiCe_{0.667}O₃ particles: sol–gel synthesis, characterization, and kinetics of photocatalytic decomposition of diazo dye – Reactive Black 5 (RB5)

Fouad Guenfoud^{a,*}, Assia Chaouche Ramdane^a, Chahrazed Belmir^a, Mutlu Sönmez-Çelebi^b

^aLaboratory of Inorganic Chemistry and Environment, Chemistry Department, Faculty of Sciences, University of Tlemcen, Tlemcen 13000, Algeria, emails: guenfoudfouad@gmail.com (F. Guenfoud), assia_chaouch_ramdane@outlook.fr (A. Chaouche Ramdane), belmirchahrazed@gmail.com (C. Belmir)

^bDepartment of Chemistry, Faculty of Science and Arts, University of Ordu, 52200 Ordu, Turkey, email: mutlucelebi@odu.edu.tr (M. Sönmez-Çelebi)

Received 20 January 2020; Accepted 10 August 2020

ABSTRACT

In order to fulfill the need for research on the synthesis of mixed oxides based on cerium and their applications in heterogeneous photocatalysis, TiCe_{0.667}O₃ powders were successfully synthesized via sol–gel technique. The phase analysis and morphology of powder particles were studied by different techniques such as X-ray diffraction, scanning electron microscopy-attached with energy dispersive X-ray spectrometry, and Fourier transform infrared spectroscopy. Brunauer–Emmett–Teller method was used for determination of specific surface area and zero point charge (pH_{pzc}). Photocatalytic activities of the particles were studied under artificial UV radiation. The influence of experimental parameters, namely, the photocatalyst concentration, initial pH, and the light energy was investigated for photodegradation of reactive dye black 5 (RB5) taken as model molecule.

Keywords: TiCe_{0.667}O₃ powders; Sol–gel method; Heterogeneous photocatalysis; Reactive Black 5 Reagent (RB5)

1. Introduction

Mixed oxides attract great attention in the fields of chemistry and solid-state physics due to their remarkable physical properties [1–4]. Currently, a large number of mixed oxides are used in catalysis studies for the development of heterogeneous catalysts in many applications such as wastewater treatment [5]. Transition metal oxides, in particular mixed oxides, have diverse properties such as thermal stability and high reactivity mainly due to their partially occupied orbitals. Moreover, they have remarkable catalytic activity in many reactions, and their low cost makes them attract great technological and industrial interest [6,7].

Most of the mixed oxides used in catalytic oxidation studies in heterogeneous systems consist of transition metals with variable oxidation states such as Ce, Ni, Ti, Fe, V,

Nb, etc. [8]. It is well-established that the properties of these materials such as reducibility, acidity, and basicity have a significant effect on the activation of reagents and that selective oxidation reactions require bifunctional properties of the solid [9].

In recent years, many oxides, mixed oxides, and supported catalysts have been the subject of academic studies to expand the field of their application to photocatalytic processes in heterogeneous phase with more or less success [1–3,10].

It is well-known that rare-earth oxides exhibit unique properties due to their unfilled 4f orbitals and lanthanide contraction. Among these rare earth elements, the amount of the cerium in the earth shell is the highest. Cerium with a 4f²5d⁰6s² electron configuration exhibits two oxidation states as +3 (Ce₂O₃) and +4 (CeO₂) [4].

* Corresponding author.

Ding et al. [5] have reported good photocatalytic activity for the mixed oxide Ce–O–Ti and successfully applied the synthesized material to catalytic ozonation for the removal of NO_x . In order to improve photocatalytic activities and reduce operating costs, more efficient catalysts must be studied. Previous articles have pointed out that one way of improving catalytic activity is doping metallic elements to catalysts like Ce–Ti [6–9,11].

However, studies on the use of cerium oxides or doped mixed oxides for catalytic reactions in liquid phase or at temperatures close to ambient remains very limited. In order to fulfill the need for new studies in this area, this work aims the synthesis of perovskite structure $\text{TiCe}_{0.667}\text{O}_3$ oxide by the sol–gel process and characterization of the oxide by different analytic techniques: X-ray diffraction (XRD), Fourier transform infrared (FTIR), scanning electron microscope (SEM), Brunauer–Emmett–Teller (BET), and zero-point charge (pH_{pzc}). Optimization of the operating conditions for heterogeneous phase photocatalysis removal using our prepared diazo type dye material has been carried out and Reactive Black 5 (RB5) was used as a model molecule.

2. Materials and methods

2.1. Materials

Isopropoxide of titanium(IV) ($\text{Ti}(\text{OCH}(\text{CH}_3)_2)_4$) and cerium(III) nitrate hexahydrate ($\text{Ce}(\text{NO}_3)_3 \cdot 6\text{H}_2\text{O}$) which were used as precursors were dissolved in water. To the precursor solutions were added citric acid ($\text{C}_6\text{H}_8\text{O}_7 \cdot \text{H}_2\text{O}$) as the complexing agent. The distilled water used for preparing the solutions and for rinsing the glassware had a pH of 6.0 and an electrical conductivity of $6.0 \mu\text{S cm}^{-1}$.

2.2. Synthesis of photocatalyst $\text{TiCe}_{0.667}\text{O}_3$ by the sol–gel process

In an Erlenmeyer flask, 1.08 g of $[\text{Ce}(\text{NO}_3)_3 \cdot 6\text{H}_2\text{O}]$ (0.002 mol) was dissolved in 12.5 mL of solvent and 0.76 mL of $[\text{Ti}(\text{OCH}(\text{CH}_3)_2)_4]$ (0.002 mol) was added. Then 1.57 g of $(\text{C}_6\text{H}_8\text{O}_7 \cdot \text{H}_2\text{O})$ (0.007 mol) was added [12]. The mixture was stirred for 6 h at room temperature leading to the formation of a gel. The gel formed was dried in the oven for 24 h at a temperature of 100°C followed by grinding to obtain a powder which will finally be calcined at $1,000^\circ\text{C}$ for 8 h with a heating rate of $10^\circ\text{C min}^{-1}$.

2.3. Photocatalytic activity of RB5

The model pollutant used in this study is reactive black 5 (RB5), which is a synthetic and anionic acid dye, widely used in the textile industry and is part of the category of azo dyes which are aromatic compounds with one or more $-\text{N}=\text{N}-$ bonds responsible for the color of the dye. Chemical structure of RB5 is given in Fig. 1.

The photocatalytic activity of $\text{TiCe}_{0.667}\text{O}_3$ catalyst was evaluated by photodegradation of RB5. All photocatalytic experiments were carried out in a 500 mL Pyrex photo-reactor with a double walled with constant stirring at room temperature under UV irradiation using a UVP Lamp pencil low mercury vapor pressure in argon, which was purchased from Pen-Ray Lamps Group Type 1115 (25 W, 18 mA, and 254 nm). The lamp was inside a quartz tube Supracil immersed in a RB5 solution with initial concentration of 50 mg L^{-1} and a volume of 500 mL.

Before the illumination, the solution was sufficiently stirred in the dark for 30 min to reach the equilibrium between the solid and the solution. At regular times of irradiation, 5 mL of RB5 solution was taken and centrifuged (10,000 rpm) to remove the catalysts. The photodegradation of RB5 was monitored by measuring the maximum absorption peak at 580 nm.

2.4. Characterizations

The crystalline structure of the samples was characterized using an X-ray diffractometer (XRD) (Rigaku-Miniflex 600, Tokyo, Japan). The diffraction patterns are recorded in 2θ in an angular range of 10° – 90° . The infrared spectra in transmission were made on a Perkin Elmer type FTIR spectrophotometer (USA). The wavelengths studied are between $4,000$ and 400 cm^{-1} . FTIR spectra were obtained using KBr pellets. The particle morphology of the material was observed using a HITACHI-TM1000, Japan scanning electron microscopy-energy dispersive X-ray spectroscopy (SEM/EDS). The BET surface area and Barrett–Joyner–Halenda (BJH) pore volume of the photocatalyst were determined by adsorption–desorption N_2 isotherm measurement at 77 K isotherms using a NOVA 1000e at the temperature of the liquid nitrogen. Prior to the analysis, we performed a degassing treatment under vacuum at 250°C overnight to remove all traces of moisture or compounds that can block

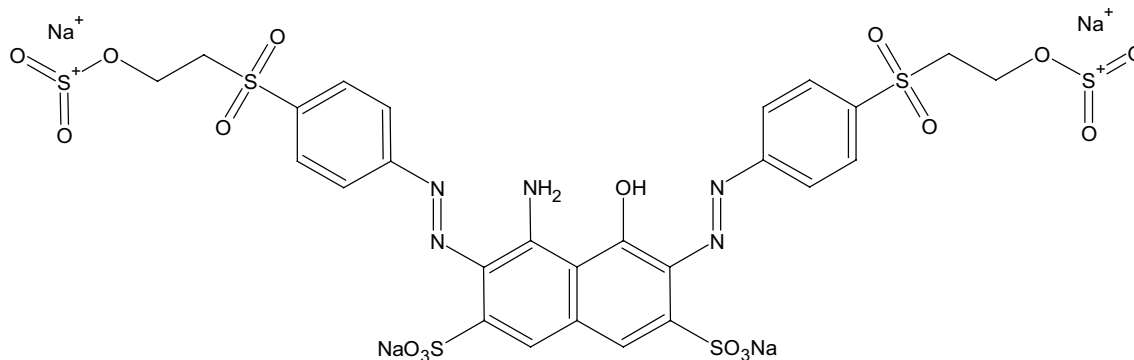


Fig. 1. Chemical structure of Reactive Black 5.

the pores of the materials. The photocatalytic activity of the catalyst was monitored using a UV-visible spectrophotometer (Perkin-Elmer, USA).

3. Results and discussions

3.1. Characterization of the $\text{TiCe}_{0.667}\text{O}_3$

3.1.1. X-ray diffraction

Fig. 2 shows the results of the XRD studies in intensity range 20–90 of the $\text{TiCe}_{0.667}\text{O}_3$ powder prepared by the sol–gel chemical process in water as a solvent and calcinated at 1,000°C. According to JCPDS01-070-3939, we have a primitive orthorhombic phase (*P*) of space group P_{mmm} with the general formula $\text{TiCe}_{0.667}\text{O}_3$, and the parameters of the mesh are $a = 3.795234 \text{ \AA}$, $b = 8.05799 \text{ \AA}$, and $c = 7.632102 \text{ \AA}$ with a mesh size $V = 110.237287 \text{ \AA}^3$. In addition, to obtaining the material $\text{TiCe}_{0.667}\text{O}_3$ and according to Fig. 2, we also have the formation of some impurities such as TiO_2 and CeO_2 .

3.1.2. Scanning electron microscopy

SEM images of $\text{TiCe}_{0.667}\text{O}_3$ particles synthesized by the sol–gel method and calcined at 1,000°C are given in Fig. 3. Characterization by scanning optical microscope allowed us to have more details on the structure as well as the morphology of the material. It should be noted that the preparation procedure has a major impact on the structure of the compound. According to the images obtained, the material obtained is of crystalline structure. Moreover, it is observed that the structure was agglomerated, the distribution is irregular, and uniform shapes are represented.

3.1.3. FTIR spectroscopy

In order to study the vibration bands of the different bonds in the material synthesized by the sol–gel pathway, the infrared spectrum of the $\text{TiCe}_{0.667}\text{O}_3$ compound prepared by sol–gel as well as the spectra of the starting precursors have been recorded (Fig. 4). Comparing spectra of the starting

precursors, that is, $\text{Ti}(\text{OCH}(\text{CH}_3)_2)_4$ and $\text{Ce}(\text{NO}_3)_3 \cdot 6\text{H}_2\text{O}$ and the spectrum of our material, we see the disappearance of the majority of the bands especially between 4,000 and 1,000 cm^{-1} , indicating that the starting materials are not found in the prepared material. A band at about 1,670 cm^{-1} was observed due to existence of the carbonyl (C=O) function of citric acid. The vibration of the metal-oxygen bond generally occurs between 1,000 and 350 cm^{-1} .

3.1.4. BET surface area and pore distribution

N_2 adsorption–desorption curves is presented in Fig. 5. All samples showed II-type isotherms based on the Brunauer–Deming–Deming–Teller (BDDT) categorization [13]. This isotherm is very widespread, for non-porous solids [13]. Table 1 shows the specific surface area (*S*) measured by the BET method, the pore volume (*V*), and the average pore diameter (*D*) $\text{TiCe}_{0.667}\text{O}_3$ calcined at 1,000°C.

3.1.5. Point of zero charge

To interpret the photocatalytic properties of the material $\text{TiCe}_{0.667}\text{O}_3$, it is interesting to know the point of zero charge (PZC) which corresponds to the state of equality between the positive charges and the negative charges on the surface of the material [14].

The presence of OH^- and H^+ ions in the solution can alter this charge potential at the surface. Hence, it is necessary to differentiate between the charge zero point and the isoelectric point (PIE). The PIE represents the charges of the external surface of the particles, whereas the PZC varies according to the net charge of the total surface (internal and external) [15]. The zero charge point is determined by different procedures depending on the electrolyte used. In our study, a solution of NaCl was used.

Determination of the zero charge point was carried out by the pH titration procedure by pouring 50 mL of NaCl solution (0.01 M) into different Erlenmeyer flasks. The pH of the solution in the Erlenmeyer flasks were adjusted from 4 to 12 by adding HCl (0.1 M) or NaOH (0.1 M). Then, 50 mg

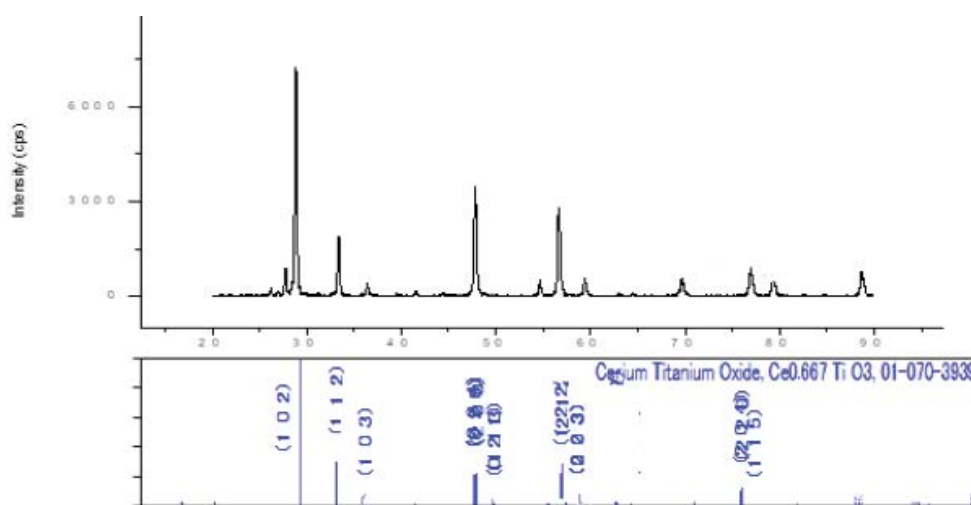


Fig. 2. XRD pattern of $\text{TiCe}_{0.667}\text{O}_3$ calcined in air at 1,000°C.

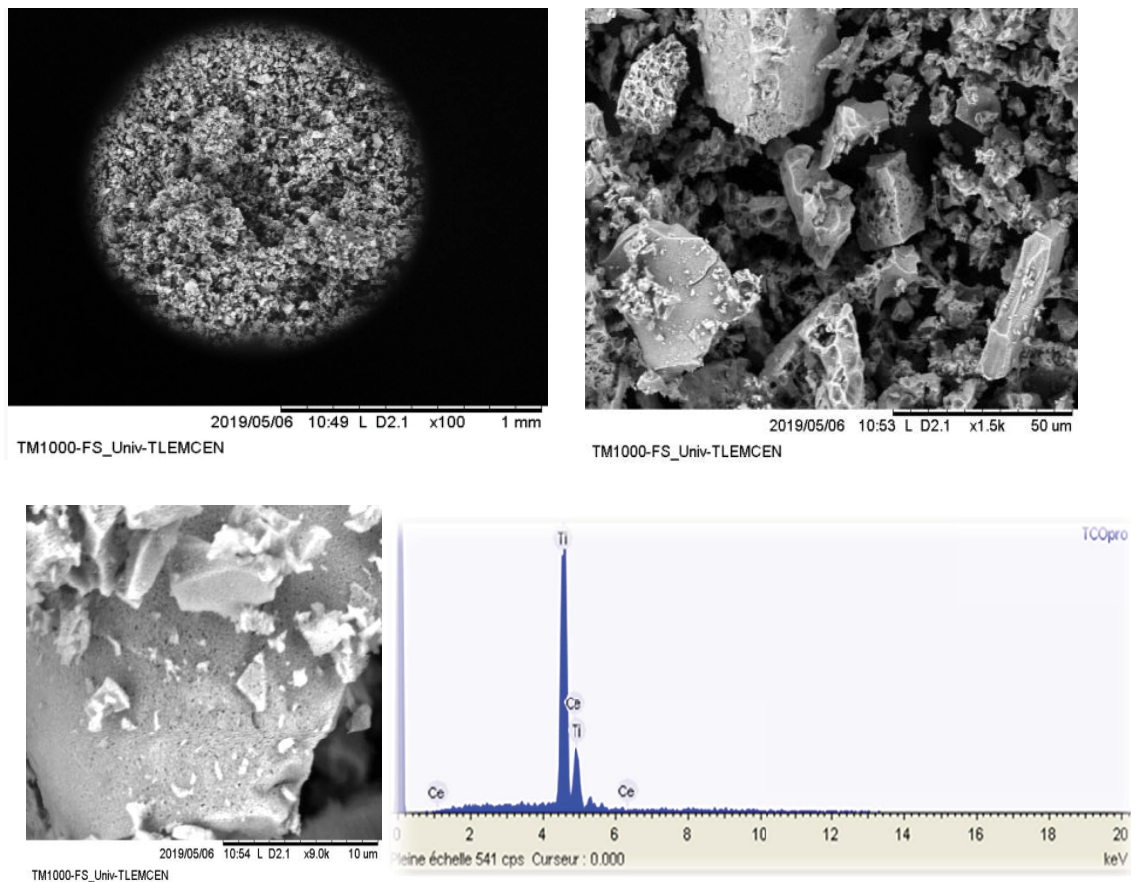


Fig. 3. SEM images of $\text{TiCe}_{0.667}\text{O}_3$ at different magnifications and the corresponding EDS spectrum.

of our material was added to each vial and the final pH was measured after 24 h. pH_{pzc} is defined as the point of intersection between the $\text{pH}_{\text{final}} - \text{pH}_{\text{initial}} = f(\text{pH}_{\text{initial}})$ and the straight line ($\Delta\text{pH} = 0$).

Fig. 6 shows the results obtained from ΔpH ($\text{pH}_{\text{final}} - \text{pH}_{\text{initial}}$) as a function of the initial pH of the material. The pH_{pzc} value of $\text{TiCe}_{0.667}\text{O}_3$ was calculated as 7.9. It can be concluded that the surface is positively charged at lower pH_{pzc} values, whereas the surface is anionic above the pH_{pzc} [15].

3.2. Study of the photocatalytic activity of $\text{TiCe}_{0.667}\text{O}_3$

3.2.1. Effect of initial pH

The pH is a parameter that affects the surface properties of solids and the state in which the pollutant will be degraded according to its pK_a . It is also a factor that characterizes the waters to be treated. Its effect on the photocatalytic activity must therefore be studied in the case of polluted water. Indeed, the dispersion of the particles and the surface charge of the catalyst are influenced by the pH of the mixture.

We studied the influence of pH on the photodegradation of the RB5 dye. The initial pH of the reaction solution was fixed by adding sulfuric acid and sodium hydroxide solutions. The evolution of the degradation of the two dyes as a function of time at the studied pH values is shown in Fig. 7. The results indicate that the photodegradation

is greater at $\text{pH} = 4$ with a yield of 94.50%. This can be explained as follows: The PZC of the $\text{TiCe}_{0.667}\text{O}_3$ obtained is equal to 7.9 (Section 3.1.5 – Point of zero charge) and thus the photocatalyst is positively charged at pH values below this and negatively charged at higher pH values. This means that at an optimal pH, which in our case is equal to 4, the surface of the photocatalyst is positively charged and since our dye is an anionic dye, attractive forces will be created leading to degradation of the pollutant [16].

3.2.2. Effect of catalyst concentration

To study the effect of the concentration of our synthesized material on the degradation of RB5, experiments were carried out in solutions prepared with distilled water in the presence of 0.06, 0.125, and 0.250 g L^{-1} of catalyst under irradiation of $\text{UV}_{254\text{nm}}$ lamp. According to the results presented in Fig. 8, when the catalyst was added in suspension to various solutions of RB5 and the reaction medium was left in the dark for 30 min, this corresponds to the abscissa negative in all cases. During this period, the results show that there is no significant removal of initial RB5 concentrations by adsorption on the photocatalyst surface in the dark. The abscissa of time $t = 0$ corresponds to the start of the exposure of the solution to the light source. This is the beginning of the photocatalysis test itself.

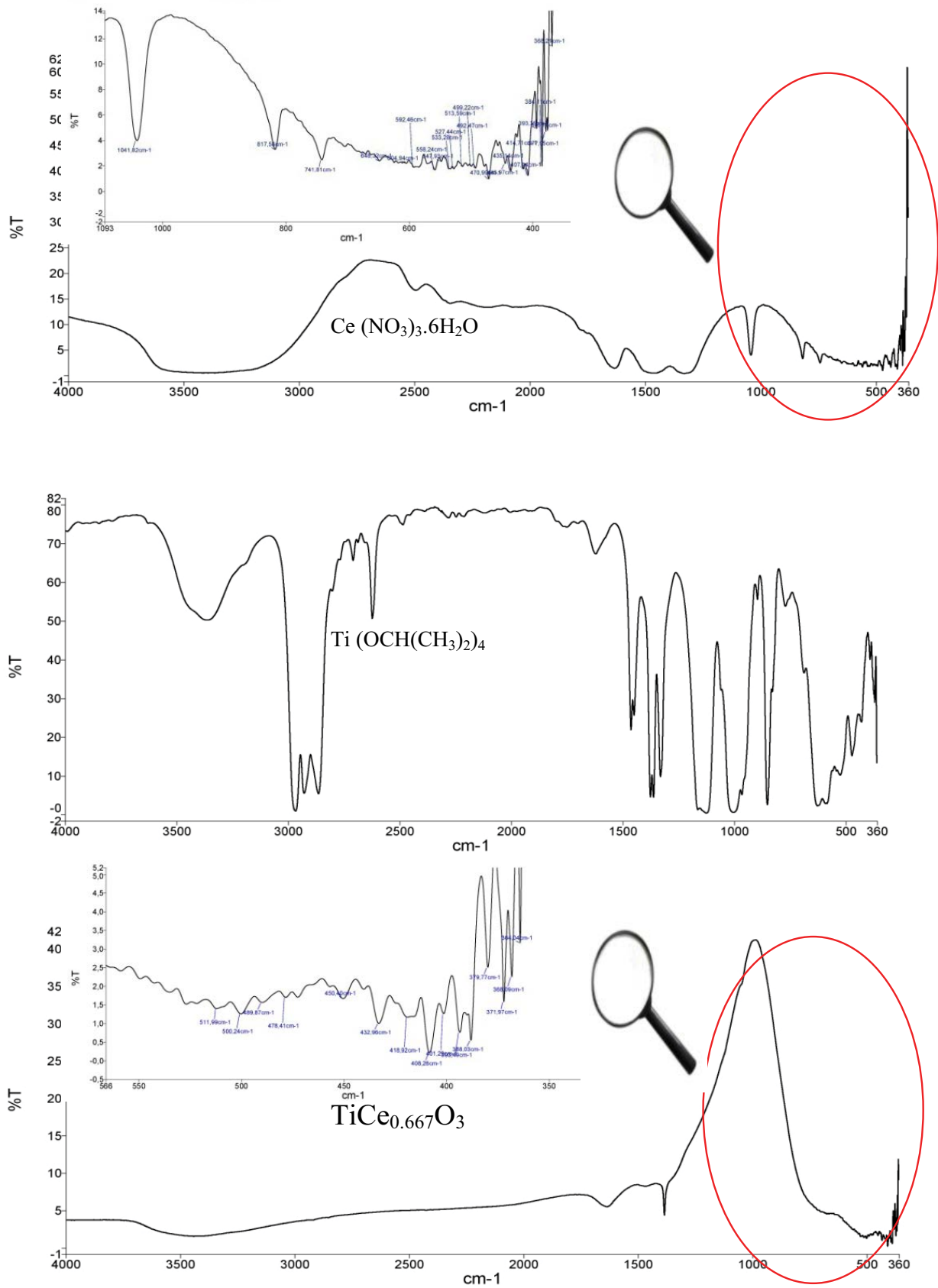


Fig. 4. FTIR spectra of precursors ($\text{Ce}(\text{NO}_3)_3 \cdot 6\text{H}_2\text{O}$ and $\text{Ti}(\text{OCH}(\text{CH}_3)_2)_4$) and the photocatalyst $\text{TiCe}_{0.667}\text{O}_3$.

Table 1
Specific surface area (S), pore volume (V), and average pore diameter (D) of $\text{TiCe}_{0.667}\text{O}_3$ calcined at $1,000^\circ\text{C}$

Photocatalyst	$\text{TiCe}_{0.667}\text{O}_3$
S ($\text{m}^2 \text{g}^{-1}$)	11.0497
V ($\text{cm}^3 \text{g}^{-1}$)	0.018430
D (nm)	48.704

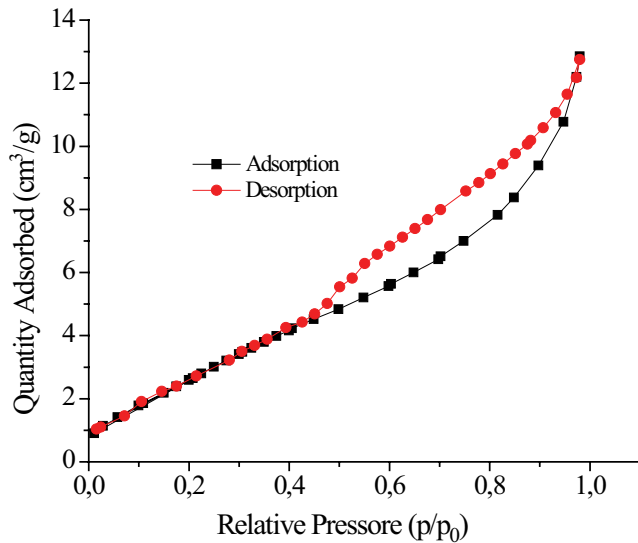


Fig. 5. Nitrogen adsorption/desorption isotherm of $\text{TiCe}_{0.667}\text{O}_3$ calcined at $1,000^\circ\text{C}$.

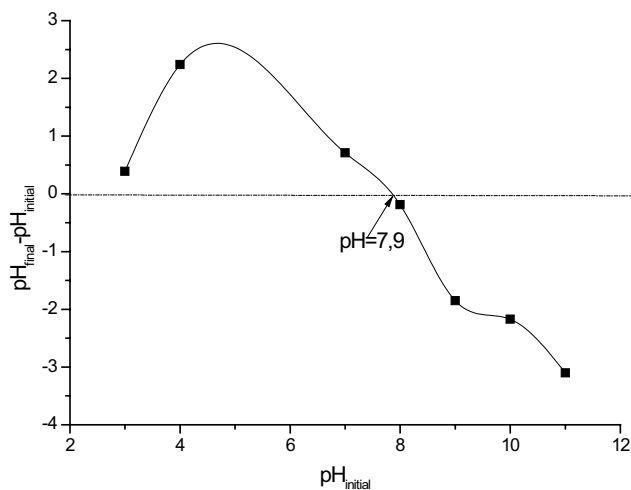


Fig. 6. Plot for the determination of pH_{pzc} of $\text{TiCe}_{0.667}\text{O}_3$.

The results reveal a rapid decrease in RB5 concentration for all concentrations of our photocatalysts.

In our case and for both materials, the best degradation occurred at a concentration of 0.06 g L^{-1} and beyond this value, there is an agglomeration of photocatalyst particles, which will make the surface unavailable [17]. A screen effect

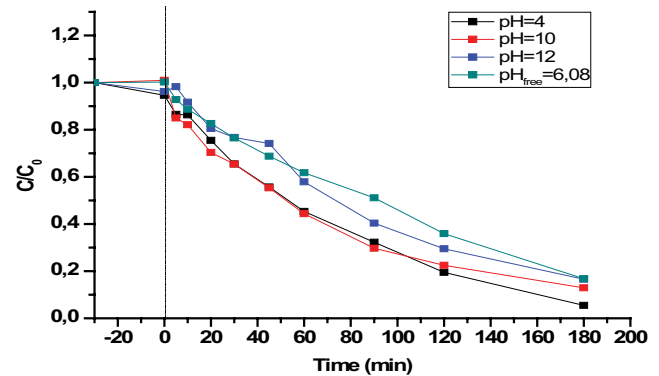


Fig. 7. Photocatalytic degradation of RB5 solution with different initial pH values.

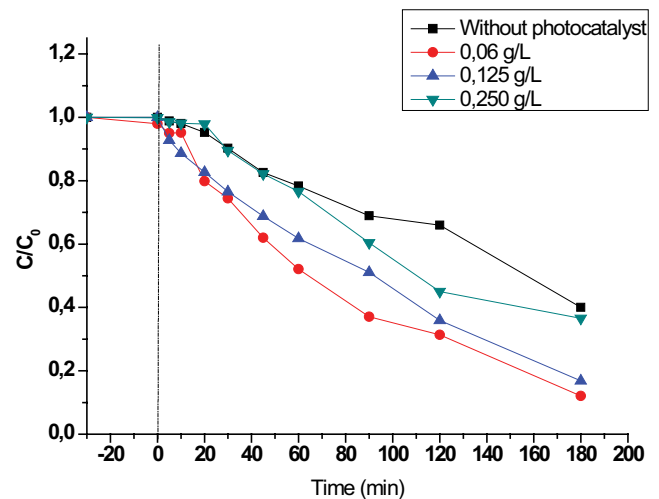


Fig. 8. Photocatalytic degradation of RB5 with different concentrations of $\text{TiCe}_{0.667}\text{O}_3$.

will occur due to excess photocatalyst and part of it will not be exposed to light leading to poor light absorption [18].

3.2.3. Kinetics and the monitoring of photodegradation by UV-vis spectrophotometer

The degradation kinetics of the RB5 studied can be expressed as follows:

$$\frac{d[\text{RB5}]}{dt} = k[\text{RB5}][\text{OH}^*] \quad (1)$$

Since the concentration of OH^* is in excess in the solution, Eq. (1) can be written as the following way:

$$\frac{d[\text{RB5}]}{dt} = k_{\text{app}}[\text{RB5}] \quad (2)$$

where k_{app} represents the apparent rate constant.

The photocatalytic decomposition of RB5 dye under optimum conditions with $\text{TiCe}_{0.667}\text{O}_3$ is gradually increasing

with increasing reaction time as seen in Fig. 9. A good linear correlation was obtained with a regression coefficient of 0.989 and pseudo-rate-constant (k) of $7.54 \times 10^{-3} \text{ min}^{-1}$ when it was fitted to a pseudo-first-order reaction (Fig. 10). The equation is given below:

$$[\text{RB5}] = [[\text{RB5}]_0] e^{-kt} \quad (3)$$

The unit of time does not depend on the initial concentrations and the knowledge of the initial concentration is not necessary to determine the rate constant k . In addition, an offset in time (e.g., $t = t' + \Delta$) does not affect the determination of the rate constant, it simply gives a different value for the initial concentration. Therefore, the rate constant can be determined for an exponential curve for which neither the initial concentration nor the initial time is precisely known. Moreover, the kinetics of the RB5 degradation was studied using the equation proposed by Gabor Lente [19]:

$$Y_t = X e^{-kt} + E \quad (4)$$

where X is the amplitude, k is the first-order rate constant, and E is the endpoint.

The integration in time is often a key question when the response time of the monitoring method is not much faster than the process studied. The integrated observation is described as [19,20]:

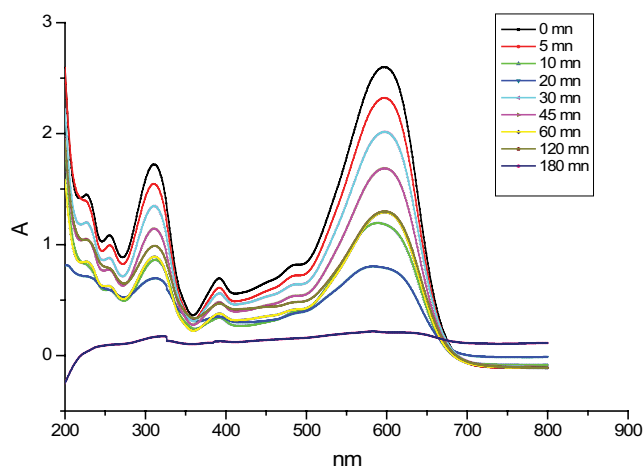


Fig. 9. UV-vis spectra of synthesized $\text{TiCe}_{0.667}\text{O}_3$ catalysts in RB5 Dye.

$$Y_t = \frac{1}{\tau} \int_t^{t+\tau} (X e^{-ks} + E) ds = \frac{1 - e^{-k\tau}}{k\tau} X e^{-kt} + E \quad (5)$$

The calculated amplitude (X), the endpoint (E), the kinetic rate constant (k), and R^2 values (coefficient of regression) are presented in Table 2. According to the Table 2, the kinetics of degradation of RB5 by the photocatalyst prepared in the work is observed for a concentration of 0.06 g L^{-1} with a rate constant equal to $9.07 \times 10^{-3} \text{ min}^{-1}$.

4. Conclusions

During this work, we managed the synthesis and characterization of perovskite type $\text{TiCe}_{0.667}\text{O}_3$ particles and studied their photocatalytic activity for degradation of RB5 as the model pollutant. We investigated the influence of experimental parameters on photocatalytic activity. To achieve our goal, we utilized the sol-gel citrate method for preparation where the prepared material was calcined at a temperature of $1,000^\circ\text{C}$. A better crystallinity of the material was obtained with a regular structure. We observed that the photocatalytic activity in the degradation of dye RB5 with UV-light irradiation reached a degradation efficiency of 100%.

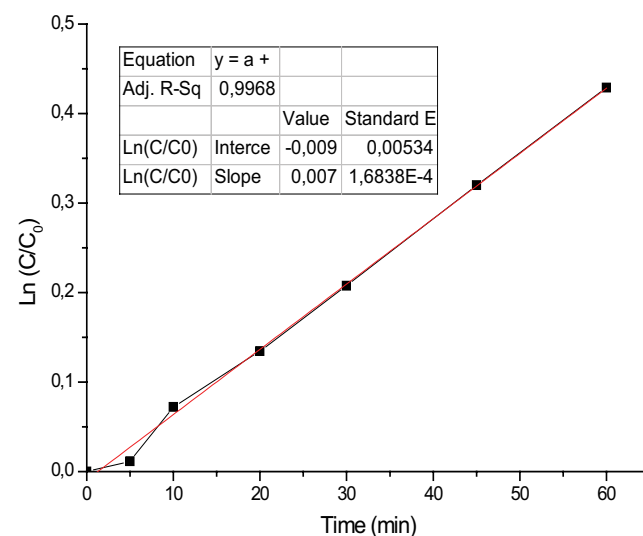


Fig. 10. Typical plot of $\ln(C/C_0)$ vs. time following pseudo-first-order reaction for photodegradation of RB5 with $\text{TiCe}_{0.667}\text{O}_3$.

Table 2
Kinetic results of degradation of RB 5

Photocatalyst (g L^{-1})	E	Standard errors	X	Standard errors	k (min^{-1})	Standard errors	R^2	Standard errors
0	4.01×10^{-5}	4.37×10^{-6}	1.07×10^{-5}	4.09×10^{-6}	4.20×10^{-2}	3.13×10^{-2}	0.954	1.86×10^{-12}
0.06	5.33×10^{-6}	5.82×10^{-6}	4.66×10^{-5}	5.39×10^{-6}	9.07×10^{-3}	2.12×10^{-3}	0.982	2.71×10^{-11}
0.125	4.30×10^{-6}	4.64×10^{-6}	4.61×10^{-5}	4.41×10^{-6}	6.53×10^{-3}	1.06×10^{-3}	0.994	5.4×10^{-12}
0.250	-7.38528×10^{-4}	8.13×10^{-3}	7.91×10^{-4}	8.13×10^{-3}	2.18×10^{-4}	2.28×10^{-3}	0.971	2.55×10^{-11}

References

- [1] M. Misono, Chapter 5 - Mixed Oxides as Catalyst Supports, M. Misono, Ed., Studies in Surface Science and Catalysis, Elsevier, 2013, pp. 157–173.
- [2] I.E. Wachs, K. Routray, Catalysis science of bulk mixed oxides, ACS Catal., 2 (2012) 1235–1246.
- [3] K. Karásková, J. Strakošová, K. Jirátová, L. Obalová, Supported Co–Mn–Al mixed oxides as catalysts for N₂O decomposition, C.R. Chim., 18 (2015) 1114–1122.
- [4] S. Liu, X. Wu, D. Weng, R. Ran, Ceria-based catalysts for soot oxidation: a review, J. Rare Earths, 33 (2015) 567–590.
- [5] J. Ding, Q. Zhong, S. Zhang, A new insight into catalytic ozonation with nanosized Ce–Ti oxides for NO_x removal: confirmation of Ce–O–Ti for active sites, Ind. Eng. Chem. Res., 54 (2015) 2012–2022.
- [6] J. Lan, M. Haneda, Z. Liu, Selective catalytic reduction of NO_x with NH₃ over a novel Co–Ce–Ti catalyst, Catal. Today, (2020), doi: 10.1016/j.cattod.2020.05.040 (in Press).
- [7] Q. Zhong, J. Ding, L. Guo, W. Zhao, S. Zhang, Effect of fluorine additives on the performance of amorphous Ce–Ti catalyst and its promotional progress on ozone for NO_x (x = 1, 2) removal at low temperature, J. Fluorine Chem., 191 (2016) 120–128.
- [8] M. Mureseanu, M. Filip, S. Somacescu, A. Baran, G. Carja, V. Parvulescu, Ce, Ti modified MCM-48 mesoporous photocatalysts: effect of the synthesis route on support and metal ion properties, Appl. Surf. Sci., 444 (2018) 235–242.
- [9] X. Cao, X. Yang, H. Li, W. Huang, X. Liu, Investigation of Ce–TiO₂ photocatalyst and its application in asphalt-based specimens for NO degradation, Constr. Build. Mater., 148 (2017) 824–832.
- [10] S. Dey, G.C. Dhal, Cerium catalysts applications in carbon monoxide oxidations, Mater. Sci. Energy Technol., 3 (2020) 6–24.
- [11] P. Ellappan, L.R. Miranda, Synthesis and characterization of cerium doped titanium catalyst for the degradation of nitrobenzene using visible light, Int. J. Photoenergy, 4 (2014) 1–9, doi: 10.1155/2014/756408.
- [12] Z. Piskula, P. Skokowski, T. Toliński, M. Zieliński, P. Kirszensztejn, W. Nowicki, Structure, magnetic and catalytic properties of SiO₂-MFe₂O₄ (M = Mn, Co, Ni, Cu) nanocomposites and their syntheses by a modified sol–gel method, Mater. Chem. Phys., 235 (2019) 121731, doi: 10.1016/j.matchemphys.2019.121731.
- [13] S. Brunauer, L.S. Deming, W.E. Deming, E. Teller, On a theory of the van der Waals adsorption of gases, J. Am. Chem. Soc., 62 (1940) 1723–1732.
- [14] M. Kosmulski, Isoelectric points and points of zero charge of metal (hydr)oxides: 50 years after Parks' review, Adv. Colloid Interface Sci., 238 (2016) 1–61.
- [15] N. Hamdi, E. Srasra, Acid-base properties of organosmectite in aqueous suspension, Appl. Clay Sci., 99 (2014) 1–6.
- [16] B. Palas, G. Ersöz, S. Atalay, Catalytic wet air oxidation of Reactive Black 5 in the presence of LaNiO₃ perovskite catalyst as a green process for azo dye removal, Chemosphere, 209 (2018) 823–830.
- [17] E.K. Goharshadi, M. Hadadian, M. Karimi, H. Azizi-Toupkanloo, Photocatalytic degradation of reactive black 5 azo dye by zinc sulfide quantum dots prepared by a sonochemical method, Mater. Sci. Semicond. Process., 16 (2013) 1109–1116.
- [18] C. Bradu, L. Frunza, N. Mihalache, S. Avramescu, M. Neață, I. Udrea, Removal of Reactive Black 5 azo dye from aqueous solutions by catalytic oxidation using CuO/Al₂O₃ and NiO/Al₂O₃, Appl. Catal., B, 96 (2010) 548–556.
- [19] H. Benbachir, H. Gaffour, M. Mokhtari, Photodegradation of 2,4,6-trichlorophenol using natural hematite modified with chloride of zirconium oxide, React. Kinet. Mech. Catal., 1 (2017) 635–653.
- [20] A. Benomara, F. Guenfoud, M. Mokhtari, Removal of methyl violet 2B by FePO₄ as photocatalyst, React. Kinet. Mech. Catal., 127 (2019) 1087–1099.